HHS Public Access

Author manuscript

Dev Dyn. Author manuscript; available in PMC 2023 August 01.

Published in final edited form as:

Dev Dyn. 2022 August ; 251(8): 1306–1321. doi:10.1002/dvdy.475.

Coordinated patterning of zebrafish caudal fin symmetry by a central and two peripheral organizers

Thomas Desvignes[1,*,†], **Amy E. Robbins**[2,*], **Andrew Z. Carey**[1], **Raisa Bailon-Zambrano**[3], **James T. Nichols**[3], **John H. Postlethwait**[1], **Kryn Stankunas**[2,†]

[1]Institute of Neuroscience, University of Oregon, Eugene OR 97403, USA

[2]Institute of Molecular Biology, University of Oregon, Eugene OR 97403, USA

[3]Department of Craniofacial Biology, University of Colorado Anschutz Medical Campus, Aurora CO 80045, USA

Abstract

Background: Caudal fin symmetry characterizes teleosts and likely contributes to their evolutionary success. However, the coordinated development and patterning of skeletal elements establishing external symmetry remains incompletely understood. We explore the spatiotemporal emergence of caudal skeletal elements in zebrafish to consider evolutionary and developmental origins of caudal fin symmetry.

Results: Transgenic reporters and skeletal staining reveal that the hypural diastema-defining gap between hypurals 2 and 3 forms early and separates progenitors of two plates of connective tissue. Two sets of central principal rays (CPRs) synchronously, sequentially, and symmetrically emerge around the diastema. The two dorsal- and ventral-most rays (peripheral principal rays, PPRs) arise independently and earlier than adjacent CPRs. Muscle and tendon markers reveal that different muscles attach to CPR and PPR sets.

Conclusions: We propose that caudal fin symmetry originates from a central organizer that establishes the hypural diastema and bi-directionally patterns surrounding tissue into two plates of connective tissue and two mirrored sets of CPRs. Further, two peripheral organizers unidirectionally specify PPRs, forming a symmetric “composite” fin derived from three fields.

[†]Corresponding authors: Thomas Desvignes, Ph.D., Institute of Neuroscience, University of Oregon, Eugene, OR 97403, Phone: 541-346-4495, tdesvign@uoregon.edu; Kryn Stankunas, Ph.D., Institute of Molecular Biology, Department of Biology, University of Oregon, 273 Onyx Bridge, 1318 Franklin Blvd, Eugene, OR 97403, Phone: 541-346-7416, kryn@uoregon.edu.

[*]Equal contributions

Authors’ contributions

Conceptualization: TD, AER, JTN, JHP, KS
Validation: TD, AER
Formal analysis: TD, AER
Investigation: TD, AER, AZC, RBZ
Resources: TD, JTN, JHP, KS
Data Curation: TD, AER
Writing – Original Draft: TD, AER, KS
Writing – Review & Editing: TD, AER, JTN, JHP, KS
Visualization: AER, TD
Supervision: TD, JHP, KS
Project administration: TD, KS
Funding acquisition: AER, JTN, JHP, KS

Distinct CPR and PPR ontogenies may represent developmental modules conferring ray identities, muscle connections, and biomechanical properties. Our model contextualizes mechanistic studies of teleost fin morphological variation.

Keywords

actinopterygian; teleosts; fin symmetry; hypural diastema; caudal fin; fin rays

Introduction

The homocercal and externally symmetric caudal fin of teleost fishes likely contributes to their evolutionary success by increasing maneuverability and thrust relative to the heterocercal and asymmetric caudal fin of most non-teleost fishes.[1–3] The teleost caudal fin skeleton comprises highly modified and often fused pre-ural and ural vertebrae, endochondral skeletal elements (i.e., haemal spines and hypurals ventrally, and epurals dorsally), and intramembranous fin rays (Fig. 1A). Fin rays, or lepidotrichia, articulate with the distal ends of endochondral elements on two “plates of connective tissue” (Fig. 1B) [4] composed of elastic cartilage.[5,6] Endochondral skeletal elements provide robust attachments to the vertebral column while rays associate with muscles and confer support and flexibility for efficient swimming. The number, types, and patterning of caudal fin endochondral elements and rays varies across species and provide diagnostic meristic characters for the classification of actinopterygian fishes (e.g., [7–10]).

Teleost homocercal caudal fins typically are externally symmetric, with equal dorsal and ventral lobes. The fin’s axis of symmetry aligns with the body axis following the upward bending of the notochord that rotates fin skeletal elements that formed earlier along the anterior-posterior body axis (e.g., [6,11–16]). The hypural diastema, a “space positioned between hypurals 2 and 3 or a notch positioned at the distal regions of hypurals 2 and 3” [10] (Fig. 1) aligns with the fin’s dorsoventral axis of symmetry and has been considered a teleost exclusivity, or synapomorphy. We previously compared teleost and non-teleost species to define the hypural diastema complex (HDC) as: 1) a gap between hypurals 2 and 3 (i.e., the hypural diastema), that 2) separates two plates of connective tissue at 3) the branching of the caudal vasculature.[6,17] Living gars have an HDC and some extinct non-teleost ray-finned fish lineages with heterocercal and asymmetric caudal fins have hypural diastemas but may lack other features of the complex. Only in teleosts, however, does the HDC align with the body axis and separate the earliest two developing caudal fin rays. Therefore, an accentuated HDC and its alignment with the body and caudal fin axes of symmetry rather than the HDC itself is likely the teleost synapomorphy. As such, external symmetry of the adult teleost caudal fin may represent an exaptation of the developmental processes forming an ancestral hypural diastema complex. [6] However, roles for HDC-associated ontogenies in the symmetrical patterning of the plates of connective tissue and the entire set of caudal fin rays in teleosts remain to be addressed.

Traditionally, teleost caudal fin rays are classified as principal or procurrent. [7] Principal rays are defined as rays supported by endoskeletal elements (i.e., hypurals, parhypural, and haemal spines of pre-ural centra 1 and 2). Principal caudal fin ray 1 is supported

by the most posterior hypural and is positioned underneath the notochord while the last principal ray (principal ray 18 in zebrafish) is the anterior-most principal ray supported by the parhypural or haemal spines of pre-ural centra 1 and 2, depending on the species (Fig. 1B). [7] Procurrent rays located along the fin's dorsal and ventral edges are shorter than principal rays, unbranched, and usually unsegmented with occasional exception of segmented posterior rays in adults. In contrast, all principal caudal fin rays are segmented and branched, except for the unbranched peripheral-most ray of each lobe referred to as the "long leading principal caudal rays" (Fig. 1, principal rays 1 and 18 in zebrafish). [7] It is largely unknown how developing rays adopt unique characteristics including their differential features and sizes associated with caudal fin symmetry.

We tracked the development of the zebrafish caudal fin endoskeleton and fin rays relative to the hypural diastema using staining methods and transgenic reporters to explore the developmental origins of teleost caudal fin symmetry. Our observations suggest that symmetry largely arises from an organizing center established at or before the onset of caudal skeleton formation and positioned at the future HDC. This proposed hypural diastema organizing center (HDOC) may pattern several elements bi-directionally and symmetrically by 1) forming the gap between hypurals 2 and 3 that 2) separates the two plates of connective tissue and 3) two sets of seven central principal rays. Further, we propose that two peripheral organizing centers (POCs) equidistant from the HDOC each pattern similar sets of two peripheral principal rays and thereby contribute to overall fin symmetry. Distinct muscle connections for the central principal rays and the two peripheral principal ray sets further reveal each set's distinctive identity, morphology, and biomechanical properties for swimming. Our model that zebrafish caudal fin symmetry originates from three organizers and responding fields contextualizes studies of caudal fin developmental mechanisms and sources of morphological variation among zebrafish genotypes and across teleost species.

Results

Zebrafish caudal fin rays emerge as mirrored sets on each side of an early-forming hypural diastema

We monitored the emergence of the zebrafish caudal fin skeleton throughout larval development using Alcian Blue and Alizarin Red staining to visualize hyaline cartilage and calcified bone, respectively. Caudal skeletal elements had not yet formed at 3.37 mm (7 dpf) (Fig. 2A). By 4.36 mm (8 dpf), the anlagen of hypurals 1, 2, and 3 had formed ventrally along the anterior-to-posterior axis (Fig. 2B). The relatively wide gap between hypurals 2 and 3 already demarcated the hypural diastema (Fig. 2B). The parhypural anlage appeared anterior to hypural 1 (Fig. 2B). At 5.27 mm (8 dpf), the parhypural began to fuse proximally with hypural 1, hypural 4 started condensing posterior to hypural 3, and haemal spine 2 formed anterior to the parhypural (Fig. 2C). Two sets of three principal caudal fin rays, faintly stained by Alcian Blue, emerged on each side of the hypural diastema (Fig. 2C, vCPR and dCPR). At 5.31 mm (8 dpf), the parhypural and hypural 1 were fused proximally (Fig. 2D, circled) and the notochord started to flex dorsally posterior to the site of contact with the parhypural and hypural 1 (Fig. 2D). Four rays were present on each side

of the hypural diastema (Fig. 2D). By 5.34 mm (9 dpf), the extending hypurals and haemal elements pivoted dorsally with the upward bending of the notochord (Fig. 2E). Ten fin rays were apparent and symmetrically arranged around the hypural diastema (Fig. 2E). At 5.50 mm (10 dpf), hypural 5 formed posterior to hypural 4 (Fig. 2F). The ten central-most rays, five on each side of the hypural diastema, were mineralized at their proximal ends as visualized by Alizarin Red (Fig. 2F). Eight additional ray anlagen – four on each side – were labelled faintly with Alcian Blue (Fig. 2F). By 5.99 mm (11 dpf), all 18 principal caudal rays showed proximal-to-distal graded mineralization (Fig. 2G). At 8.44 mm (15 dpf), four of each ventral and dorsal procurrent rays were present and mineralized (Fig. 2H). These results show that zebrafish caudal fin endochondral elements form earlier than caudal fin rays but without obvious dorsoventral symmetry. In contrast, fin rays are symmetrically arranged throughout caudal fin development, emerging as dorsal and ventral mirrored sets on each side of an early-forming hypural diastema.

Two plates of connective tissue develop symmetrically from twin cartilage precursor pools on each side of the hypural diastema

The two “plates of connective tissue” [4] at the junction between caudal fin endochondral elements and bony rays also develop symmetrically on each side of the hypural diastema. We followed their formation using cartilage-marking transgenic reporters derived from *sox10*, *trps1*, and *sox9a* regulatory sequences. The transgenic line *sox10:mRFP* labels cell membranes within caudal fin endochondral skeletal elements (e.g., haemal spines and hypurals) (Fig. 3A–E). [18] The *trps1:EGFP* transgene marks joint precursor cells and skeletal joints. [19] Double transgenic *sox10:mRFP;trps1:EGFP* fish showed specific *trps1*-driven GFP in precursor cells of the plates of connective tissue at the distal epiphyses of mRFP-positive hypurals and haemal spines (Fig. 3A–F). Two patches of *trps1:EGFP*-expressing progenitor cells first appeared on each side of the hypural diastema at the epiphyses of hypurals 2 and 3 at ~4.80 mm (7 dpf) (Fig. 3A, white arrows in A’). The two differentiating plates of connective tissue remained distinct at ~5.45 mm (9 dpf, Fig. 3B, B’). The anterior plate spanned the epiphyses of the parhypural and hypurals 1 and 2 (Fig. 3B, B’), while the posterior plate extended across the epiphyses of hypurals 3 and 4 (Fig. 3B, B’). At later stages, each cartilaginous plate condensed where proximal endochondral skeletal elements (haemal spine 2, parhypural, and hypurals 1 and 2 for the ventral plate, and hypurals 3 to 5 for the dorsal plate) articulated with distal principal caudal fin rays (Fig. 3C–F).

We combined the *sox10:mRFP* transgene with the pan-cartilage marker *sox9a:EGFP* [20] to further resolve plates of connective tissue formation. Expression of *sox9a:EGFP* reinforced the plates’ cartilaginous nature and their distinct ontogenies on each side of the hypural diastema (Fig. 3G–H). The combination of *sox10* and *sox9a* reporters further revealed differences in cartilage subtypes. The *sox10* and *sox9a* reporters were co-expressed in endochondral skeletal elements (i.e., haemal spine, parhypural, and hypurals) made of hyaline cartilage, while only *sox9a:EGFP* was expressed in the plates of connective tissue (Fig. 3G–H) made of elastic cartilage. [5,6] The *sox9a:EGFP* expression pattern in the developing caudal fin thus corresponds to the combined *sox10:mRFP* and *trps1:EGFP* expression patterns. Together, we conclude that cartilaginous plates of connective tissue

emerge independently from one another and distal to endochondral skeletal elements from twin precursor pools located on each side of the hypural diastema.

Transgenic markers show distinct emergence of two sets of two peripheral principal rays

We used the transgenic markers *RUNX2:mCherry* [21] (from S. Fisher lab) and *sp7:EGFP* [22] to follow the pattern of emergence of caudal fin rays in individual larvae starting at 4.57 mm (8 dpf). Pre-osteoblasts express *runx2*, differentiating osteoblasts strongly express both *runx2* and *sp7*, and mature osteoblasts express *sp7* with decreased *runx2* expression. [23–25] Hence, *RUNX2:mCherry* and *sp7:EGFP* double reporter fish enable tracking osteoblast states and transitions prior to ray calcification. We first observed *RUNX2:mCherry* expression at 4.57 mm (8 dpf) in two developing principal caudal fin rays, one on each side of the hypural diastema (Fig. 4A). These rays would become the central-most rays 9 and 10 of the adult fin (see Fig. 1, Video S1). Ten hours later, at 4.60 mm (8.5 dpf), a second mirrored pair of *RUNX2:mCherry*-expressing rays emerged while the first pair now co-expressed *sp7:EGFP* proximally, indicating initial pre-osteoblast differentiation (Fig. 4B). At 5.21 mm (9 dpf), four mirrored pairs of rays had formed with the inner two pairs co-expressing *RUNX2:mCherry* and *sp7:EGFP* (Fig. 4C). By 5.42 mm (9 dpf), five mirrored pairs of principal rays symmetrically emerged around the hypural diastema. The central-most six rays, three on each side, co-expressed *RUNX2:mCherry* and *sp7:EGFP* proximally while *RUNX2:mCherry* single positive pre-osteoblasts were restricted to the most recently added principal rays and the distal ends of all developing rays (Fig. 4D, Video S1).

At 5.56 mm, principal ray 2 and principal ray 17 emerged simultaneously but asynchronously from the central group of principal rays and with a notable gap separating each from the central ray field (Fig. 4E–E”, Video S1). These separate rays and the most recently developed mirrored pair of now 10 central rays (rays 5 and 14) expressed *RUNX2:mCherry* but not *sp7:EGFP* (Fig. 4E–E”). A few *RUNX2:mCherry*-expressing precursors of principal ray 18 also appeared anterior to principal ray 17 (Fig. 4E–E’). By 5.71 mm, a sixth mirrored pair of central principal rays and principal ray 1 emerged (Fig. 4F–F”). The four peripheral rays (principal rays 1, 2, 17 and 18), organized as dorsal and ventral sets of two rays each, remained distinctly separated from the central principal ray field, which now comprised rays 4 to 15 (Fig. 4F–F”, Video S1). Rays 2, 5, and 14 now co-expressed *RUNX2:mCherry* and *sp7:EGFP* (Fig. 4F, F”). By 5.99 mm, all 18 principal rays were present (Fig. 4G–G”, Video S1). The last rays to emerge, mirrored central principal rays 3 and 16, were slightly shorter than their respective flanking rays (Fig. 4G–G”). By 6.01 mm, the continuous, fan-like caudal fin comprised 18 outgrowing rays, segmented by joints, mirrored on dorsal and ventral lobes, and centered around the hypural diastema (Fig. 4H–H”, Video S1). Thus, while central principal rays (CPRs, rays 3-16) emerge synchronously, sequentially, and symmetrically by mirrored pairs around the hypural diastema, peripheral principal rays (PPRs, rays 1-2 and 17-18) emerge independently and earlier than adjacent CPRs (rays 3, 4, 15 and 16). PPRs, like CPRs, emerge in outward progression.

To further discern the developmental mechanisms of peripheral and central principal rays, we used the transgenic line *alx4a:DsRed2,* which expresses a red fluorescent reporter in fin fibroblasts and osteoblasts in position-specific manners, including in the anterior-most rays of paired and median fins. [26] In adults, *alx4a:DsRed2* is distinctly expressed in the ventral-most caudal fin ray, but its pattern has not been described throughout caudal fin development. [26] At 4.43 mm (9 dpf), the fin fold had not yet developed rays and expressed *alx4a* mostly in iridophore pigment cells (Fig. 5A). [27] By 5.41 mm (12 dpf), we observed strong *alx4a:DsRed2* expression at the posterior end of the ventral melanophore stripe before the caudal fin condensation region (Fig. 5B) [28] and faint expression just below the notochord distal tip (Fig. 5B, white arrowhead). By 5.74 mm (13 dpf), ventral and dorsal *alx4a:DsRed2* expression intensity increased (Fig. 5C). By 5.97 mm (14 dpf), dorsal *alx4a:DsRed2* expanded along the length of developing principal rays 1, 17, and 18, and faintly at the base of ray 2 (Fig. 5D, yellow arrowheads). At 6.48 mm (15 dpf), *alx4a:DsRed2* was clearly expressed in principal rays 1-2 and 17-18 (Fig. 5E, yellow arrowheads) and in the developing ventral and dorsal procurrent ray regions (Fig. 5E, orange brackets and arrowheads). The *alx4a:DsRed2* was also expressed along the leading peripheral rays of the emerging dorsal and anal fins, consistent with a previous report [26] (Fig. 5E, green and blue arrows). At 6.80 mm (16 dpf), *alx4a:DsRed2* expression persisted along each peripheral-most principal ray (rays 1 and 18) and in the developing ventral and dorsal procurrent ray regions but was now faint along principal rays 2 and 17 (Fig. 5F, yellow arrowheads). The *alx4a:DsRed2* also became visible in emerging ray joints (Fig. 5F, yellow dashed zoom box). By 8.69 mm (21 dpf), *alx4a:DsRed2* was expressed most intensely in peripheral principal rays 1 and 18, was present but more muted in rays 2 and 17 (Fig. 5G, G' yellow arrowheads), highly expressed in dorsal and ventral procurrent rays (Fig. 5G, G' orange brackets), and remained restricted to the ray joints in central principal rays (Fig. 5G, G', dashed yellow zoom inset). Only later, in reproductive adults, did *alx4a:DsRed2* expression become mainly restricted to the ventral-most peripheral principal ray 18, as previously reported (data not shown). [26] Expression of *alx4a:DsRed2* restricted to developing PPRs (and procurrent rays) reinforces the conclusion that the PPRs have different developmental mechanisms, and potential different identities, compared to the symmetrically-emerging CPRs.

Each set of central and peripheral principal rays associates with distinct caudal muscles

Caudal fin rays attach to the caudal muscles conferring thrust and maneuverability during swimming. We explored if ray symmetry was reflected in musculoskeletal attachments by combining muscle staining with transgenic markers. Phalloidin staining of actin filaments (F-actin) in ~8.00 mm *alx4a:DsRed2* fish (27 dpf) showed that inerfilamenti caudalis dorsalis (ICD) and inerfilamenti caudalis ventralis (ICV) muscles connected to central principal rays (rays 3-16) but not to *alx4a:dsRed2*-expressing peripheral principal rays (rays 1-2 and 17-18) (Fig. 6A, A'). [29] Confirming previous observations, [30,31] the tendon-labeling *scxa:mCherry* line [32] was expressed strongly in myosepta between myomeres and at caudal fin ray joints (Fig. 6B, B'). In addition, we observed robust *scxa:mCherry* expression along a proximal stretch of all principal and procurrent fin rays, reinforcing that caudal musculature anchors to the base of all fin rays (Fig. 6B–B'). Finally, the proximal, central ends of ICD and ICV appeared attached to rays 7-9 and 10-12, respectively while the distal, peripheral

ends of ICD and ICV associated with rays 3-6 and 13-16, respectively (Fig. 6A–A', C). This ICD and ICV attachment pattern to CPRs may confer undulating movement capacities. These studies demonstrate that the ICD and ICV muscles attach to the central principal rays 3 to 16 with a matching symmetrical arrangement around the hypural diastema. [29]

Myosin heavy chain (Mhc) staining of *sp7:EGFP* fish further highlighted the symmetric organization of similarly shaped ICD and ICV muscles around the hypural diastema and their attachment to respective dorsal and ventral central ray sets (Fig. 6C–D). Dorsally, the adductor caudalis ventralis (ACV) attached to the base of peripheral principal rays 1 and 2 (Fig. 6D, E). [29] Ventrally, the flexor caudalis ventralis superior (sFCV) attached to the base of peripheral principal rays 17 and 18. Further, the flexor caudalis ventralis inferior (iFCV) attached to the base of ventral procurrent rays (Fig. 6D, F). [29] Together, these observations reveal that dorsal and ventral sets of central rays and both peripheral principal ray sets attach to distinct caudal muscles. Fin symmetry extends to the pairing of mirrored ICD and ICV muscles with respective dorsal and ventral CPR sets on each side of the hypural diastema. In contrast, muscles attached to the dorsal and ventral peripheral principal rays are not symmetrically organized and display morphological differences in shape, length, and ray attachments.

Discussion

Our study of the emergence of zebrafish caudal fin skeletal elements from progenitor cell states reveals potential patterning mechanisms underlying external fin symmetry of adults. Our results indicate that caudal fin symmetry largely arises from the synchronous emergence of mirrored sets of central principal rays (CPRs) forming around an early-developing hypural diastema – the gap between hypurals 2 and 3 at the caudal fin's dorsoventral axis of symmetry (Fig. 7). Similarly, the two plates of connective tissue develop symmetrically around the hypural diastema. In contrast, the two peripheral principal rays (PPRs) of each fin lobe develop asynchronously from the central principal rays. Each CPR and PPR set also connects to distinct swimming muscles. Collectively, we propose that zebrafish fin symmetry arises from the action of three organizers: a central hypural diastema organizing center (HDOC) and two peripheral organizing centers (POC). By this model, the HDOC patterns the surrounding field bi-directionally into mirrored plates of connective tissue and sets of CPRs. The two POCs, spaced equidistant from the HDOC along the anterior-posterior body axis, form sets of two PPRs each. By this model, the caudal fin composite appendage is assembled from at least three organizers and responding fields, defining developmental modules. Unique anterior-posterior-defined positional identities of each module could confer distinct muscle attachments, ray morphologies, and growth properties to each ray set for optimized fin shape, swimming biomechanics, and life history traits. Further, genetic changes affecting one module or another could explain symmetry-breaking morphological variations observed in several teleost groups.

The hypural diastema reflects an early developmental organizing center that determines the axis of external symmetry of the adult zebrafish caudal fin

Endoskeletal caudal fin elements do not develop symmetrically and the earliest forming elements (i.e., the two hypurals H1 and H2) are located anterior to the future hypural diastema so that the diastema becomes visible only when hypural 3 initially forms posterior to it, as previously described. [5,6,33] Therefore, an HDOC influence on endoskeletal elements would appear restricted to establishing the extra space between hypurals 2 and 3. Instead, endoskeletal element emergence and morphogenesis likely is regulated by distinct regulatory modules, potentially including antero-posterior patterning genes (e.g., *hox* genes) and hedgehog signaling. [34] In contrast, we propose that an HDOC regulates the symmetrical emergence of distal caudal fin skeletal elements. Plates of connective tissue develop distal to the endochondral elements, forming elastic cartilage joints at the articulation between the endochondral elements and fin rays in the adult caudal fin. [5,6] The ventral plate of connective tissue spans haemal spine 2, the parhypural, and hypurals 1 and 2. The dorsal plate of connective tissue spans hypurals 3 to 5. The *trps1* and *sox9a* transgenic lines demonstrate that the two plates of connective tissue develop simultaneously but separately and persist as two independent plates through adulthood. Thus, we propose that the HDOC patterns both plates of connective tissue and maintains their separation. Our muscle staining, matching a developmental series of zebrafish caudal muscle formation, [29] shows that ICD and ICV caudal muscles also develop symmetrically on each side of the hypural diastema in association with respective dorsal and ventral CPRs and thus may also be patterned by the HDOC. In addition, the HDOC may also influence the branching of the caudal vasculature and caudal nerve axons that each ramify dorsally and ventrally at the hypural diastema. [4,6,35] Together, the HDOC likely broadly patterns the surrounding mesoderm and its innervating axons.

We propose that the central HDOC also drives the symmetric patterning of the CPRs. Mirrored CPRs emerge synchronously and symmetrically on each side of the hypural diastema, consistent with previous observations in zebrafish [6,28] and medaka. [36] Thus, the HDOC may be a source of unknown morphogens that bidirectionally and progressively specify ray emergence, befitting our proposed “organizer” designation. Further, the regularly-spaced specification of ray pre-osteoblasts in a stripe-like pattern suggests a Turing reaction/diffusion process, as proposed for a Bmp-Sox9-Wnt network in tetrapod limb and pectoral fin endoskeleton patterning. [37,38] Greater distance from the HDOC correlates with larger and longer rays. This pattern could reflect morphogen-specified, differential ray outgrowth properties (e.g., population sizes or cell-level positional identities). Regardless, the HDOC seemingly patterns 14 of the 18 principal rays and establishes much of external caudal fin symmetry, including the axis of symmetry. Meanwhile, the upward bending of the notochord rotates the anterior-posterior specified appendage into its caudal position in dorsoventral alignment with the body axis.

Two early-forming peripheral organizing centers may pattern the caudal fin peripheral rays

Our time course monitoring *RUNX2:mCherry*-expressing pre-osteoblasts tracks the earliest onset of caudal fin ray emergence. Notably, in all observed specimens across many clutches, rays 1-2 and 17-18 emerge separately from rays 3-16 and earlier than neighboring CPRs

(rays 3, 4 and 15, 16) within a 24-hour period from 9-10 dpf (5.5-5.7 mm). The neighboring CPRs (rays 3, 4 and 15, 16) then quickly bridge the gaps such that the separate emergence of the peripheral rays is no longer apparent. We call these rays (1, 2, 17, and 18) peripheral principal rays (PPRs) as a subtype of principal caudal fin ray ontogenetically distinct from the CPRs. The lag between osteoblast specification and tissue mineralization likely prevented detection of this ray emergence pattern in earlier studies (e.g., [5,6,11,28]). Principal rays therefore develop in one of three groups separated by developmental time and anterior-posterior body axis position – the central CPRs plus what become dorsal and ventral sets of PPRs.

Expression of an *alx4a*-driven transgene shows that all four developing PPRs express a distinct transcription factor from the CPRs, reinforcing the different ontogeny and potential identities of PPRs compared to CPRs. Further, *alx4a:DsRed2* expression at the site of the later-developing ventral PPRs (vPPRs) predates the appearance of *RUNX2:mCherry*-expressing PPR pre-osteoblasts. Likewise, but later in development, *alx4a:DsRed2* expression at the site of the future dorsal PPRs (dPPRs) precedes the emergence of *RUNX2:mCherry*-marked corresponding PPRs. Therefore, the caudal mesenchyme fields forming PPRs may be distinct from that of the CPRs. We favor a model whereby peripheral organizing centers (POCs) within these fields specify the two peripheral-most principal rays of each caudal fin lobe. In contrast, a single organizing center (the HDOC) seems unlikely to produce developmentally staggered waves of rays, unless mesenchymal cells at the future PPRs differentiate under lower levels of a hypothetical HDOC-originating morphogen. The temporal delay between the establishment of the vPOC (more anterior) and dPOC (posterior) may reflect the progressive anterior-posterior differentiation of caudal mesenchyme, as seen with endochondral elements. POCs may limit the number of principal rays by restricting the continued bi-directional advance of sequentially forming central rays. Later developing procurrent rays also may be specified by the POCs or by additional, procurrent ray-specific organizers. These hypotheses tying organizers to sets of rays (e.g., the HDOC to all CPRs) with cross-organizer interfering effects could be tested by combinatorial transplantations and ablations of to-be-identified HDOC and POC cells prior to ray emergence.

The formation of two POCs approximately equal distance from the HDOC along the anterior-posterior body axis seemingly is necessary for overall adult fin symmetry. Further, the POCs appear largely equivalent given they produce the same number of PPRs with each mirrored pair of approximately equal length and morphology. Small deviations in POC position, timing of emergence, or potency relative to the HDOC would readily explain the occasional variation in numbers of principal rays in zebrafish ventral and dorsal caudal fin lobes. [11,28] Ray radius measurements indicate PPRs are proportionately wider than CPRs. [39] Therefore, PPR-comprising cells may have distinct growth properties reflective of independent ontogenies and potentially different positional identities. CPR, vPPR, and dPPR positional identities, shared across cells comprising each set of rays and established by anterior-posterior body axis position, could then influence regenerative responses that robustly restore the caudal fin's homocercal and externally symmetry shape even following diagonal or other asymmetric amputations. Regardless, all three organizers would have to

be precisely “tuned” to collectively provide external fin symmetry – a teleost innovation seemingly under strong selective pressure.

Distinct muscles attach to central and peripheral principal caudal fin ray sets

The different ontogeny, morphology, and positional identity of CPRs and PPRs likely underlie different biomechanical roles for each principal caudal fin ray type. Transgenic *alx4a* expression, thought to label a subset of fibroblasts, osteoblasts, and/or ligaments, [26,40] and tendon marker *scxa* [32] combined with myosin heavy chain and phalloidin muscle staining reveal that CPRs and PPRs connect to different caudal swimming muscles. [2,41,42] CPRs attach to inerfilamenti caudalis dorsalis (ICD) and inerfilamenti caudalis ventralis (ICV) muscles that develop and are positioned symmetrically around the hypural diastema. [29] In contrast, dPPRs and vPPRs associate with the peripheral abductor caudalis ventralis (ACV) and superior flexor caudalis ventralis (sFCV) muscles, respectively. Therefore, different muscles can independently move the ventral PPRs, dorsal PPRs, and both CPR sets, contributing to complex swimming dynamics. [1,3,42] The most peripheral, sturdier, and unbranched PPRs (principal rays 1 and 18) likely provide stiffness to the caudal fin by framing the ray field to enhance caudal fin thrust. Indeed, in fluid-structure interaction models, a “cupping” stiffness pattern for caudal fins (similar to the pattern seen in zebrafish; highest rigidity at the boundaries and lowest in the center) requires the least energy expenditures to generate the largest thrust. [43–45] Similar to the observed muscle-to-ray set pairings, PPRs and CPRs show distinct innervation. [35] Together, the different ontogeny of PPRs and CPRs under the control of three organizing centers may provide each ray set with distinct identities altering ray morphology as well as muscle and nerve targeting, collectively optimizing biomechanical properties for efficient thrust and maneuverability.

Evolutionary conservation of caudal fin organization

Our model that an HDOC and two POCs pattern the symmetric zebrafish caudal fin suggests that similar organizers are conserved across teleosts with externally symmetric fins and that altered organizers underlie symmetry-breaking forms. Further, our model raises questions about the organizers’ evolutionary origins and lineage-specific variations. While not specifically observed in the ontogeny of all teleost species, the hypural diastema defined as a gap between hypural 2 and 3 or a notch between hypural plates is a teleost hallmark, [8,46] although also observed in gars. [6,17] Further, in documented teleost species, the sequential and symmetrical emergence of CPRs around the hypural diastema appears to be conserved (e.g., [6,12–16,47]). In contrast, in spotted gar, the first rays to form are not located around the hypural diastema but instead adjacent to hypurals 1 and 2. [6] In both gars and teleosts, however, the gap between hypural 2 and 3 coincides with the separation of the connective tissue plates and the branching of the caudal vasculature. [6] Therefore, an HDOC may pattern the hypural diastema, each plate of connective tissue, and the caudal vasculature in both gars and teleosts. As such, the exaptation of an HDOC to additionally pattern CPRs and establish external symmetry may be a synapomorphy of the teleost group, extending our previous hypothesis. [6] Alternatively, the putative gar HDOC may pattern surrounding rays but without symmetry due to uneven bi-directional morphogens, pre-existing field asymmetry in size or cell sensitivity to diffusible morphogens, or the interference of nearby ray organizing centers. Additional targeted work on non-teleost actinopterygians is needed to evaluate the

relationship of our hypothesized teleost HDOC to other hypothesized actinopterygian 'tail' organizers. [48]

Studying the conservation of PPRs and POCs across teleost and non-teleost species is difficult because traditional methods such as Alcian Blue and Alizarin Red stain differentiated tissue rather than progenitor cells. However, in teleosts, a similar pattern of asynchronous emergence of CPRs and PPRs in goldfish detected using calcein to label forming bones (Figs. 22 and 33 in [15]) suggests conservation of POCs among cyprinids. Transgenic reporter lines and molecular labeling techniques in other teleost and non-teleost fish groups would further explore the conservation of PPRs, and thus likely POCs, and reveal their evolutionary origin as an ancestral ray-finned fish character, a teleost innovation, or a derived character in some teleost lineages. Nonetheless, we hypothesize that altered POC modules could explain strikingly asymmetric caudal fin forms. For example, the ornamental sword of male swordtail *Xiphophorus* spp. contributing to mate choice is characterized by disproportionately extended ventral PPRs. [49] Thus, the hypothesized *Xiphophorus* "sword organizer" [50,51] may correspond to the zebrafish ventral peripheral organizing center (vPOC) and confer distinct growth properties to ventral PPRs. The elongation of dorsal PPRs in female swordtails treated with testosterone [50] suggests the conservation of the dorsal POC and its relatedness with the vPOC. Flying fishes and tripodfishes (*Bathypterois* spp.) also have dramatically elongated ventral caudal fin lobes, again with particularly long ventral PPRs possibly specified by a specialized vPOC. In flying fishes, elongated ventral PPRs enable propulsion while the rest of the body is out of the water. [52] In tripodfishes, the extremely long caudal fin ventral PPRs that match pelvic fin ray length enable a posture parallel to the substrate. [53] Altered POC modules may also drive the remarkable extension of the peripheral-most principal caudal fin rays of some whiptail catfishes (Loricariinae) (e.g., [54–57]). Co-characterizing caudal fin ray ontogeny, morphologies, and muscle attachments in these groups would help elucidate if and how changes to vPOC/vPPR modules cause caudal fin symmetry-breaking and ray elongation phenotypes.

Studies identifying the genetic mechanisms underlying PPR elongation can inform on the specificity of POC modules. The elongated rays of the swordtail *Xiphophorus helleri*'s ventral caudal fin lobe are promoted by the potassium channel *kcnh8*, [51] a paralog of *kcnh2a*, of which ectopic expression causes dramatic fin ray overgrowth in *longfin*^{t2} (*lof*^{dt2}) mutant zebrafish. [58,59] Similarly, the *kcnk5a* and *kcnk9* potassium channels may promote ventral lobe elongation in flying fish caudal fins. [58] Gain-of-function mutations in the related potassium channel *kcnk5b* extend fin rays of the zebrafish *another longfin* (*alf*) mutant [60] and cause the *long-tail* phenotype in goldfish. [61] Overexpression of additional potassium channels also cause zebrafish caudal fin overgrowth. [62] Therefore, organizer- or field-specific variations in ion channel expression could readily alter fin morphology under evolutionary selection. Expression studies of potassium channel genes and downstream ion signaling driving teleost caudal fin variation will help decipher these evolutionary and ray outgrowth mechanisms. Genetic changes that add, remove, or reposition organizers and alter their developmental influence could produce additional types of symmetry-breaking caudal fin forms. Collectively, our model provides a framework to explore the existence and

function of developmental organizers in the caudal and other fins and their roles in fin shape evolution.

Experimental Procedures

Zebrafish lines

Zebrafish (*Danio rerio*) were maintained in 28-29°C circulating fish water within the University of Oregon Aquatic Animal Care Services (UO AqACS) fish facility and the University of Colorado Anschutz Medical Campus. The following lines were used: wildtype AB, *Tg(trps1:EGFP)*^{i1271aGt}, [19] *Tg(sox10:mRFP)*^{vu234}, [18] *Tg(sox9a:EGFP)*^{zc81Tg}, [20] *Tg(RUNX2:mCherry)* (Shannon Fisher Lab, [21]), *Tg(sp7:EGFP)*^{b1212}, [22] *Tg(alx4a:DsRed2)*^{pd52}, [26] and *Tg(scxa:mCherry)*^{fb301Tg}. [32] Zebrafish experiments were approved by the Institutional Animal Care and Use Committees (IACUC) of the University of Oregon and the University of Colorado Anschutz Medical Campus.

Zebrafish developmental stages are described primarily by standard length (SL). SL was measured using ImageJ [63] from the snout to the tip of the notochord in pre-flexion larvae and from the snout to the caudal peduncle in post-flexion larvae. The age of all animals is also reported as days post fertilization (dpf). However, some discrepancies in SL and dpf exist between fish lines because fish were reared in different facilities with differing developmental rates. SL could not always be accurately measured by stereomicroscopy for older, larger specimens. In these instances, SL (denoted by ~) was estimated based on skeletal element development, pigmentation patterns, and degree of notochordal flexion. [28,64]

Alcian Blue and Alizarin Red staining

Briefly, fish were euthanized with an overdose of MS-222 (Syndel), fixed in 4% paraformaldehyde (PFA), washed, and serially transferred into 80% ethanol for storage or immediate staining. Fish were stained first with Alcian Blue for cartilage, enzymatically cleared using 1% trypsin, bleached in 3% hydrogen peroxide, differentially stained with Alizarin Red for calcified bone, and finally cleared with increasingly concentrated glycerol solutions. [17,65] Specimens of various sizes were prepared and stained following the same method but the length of each step was adjusted according to the size of the fish.

Whole mount fluorescent staining

Fish were euthanized by MS-222 overdose, fixed in 4% PFA, and washed in PBS. Phalloidin staining (AlexaFluor 647 Phalloidin, Thermo Fisher #A22287) was performed at 1:1000 in PBS + 0.1% Triton X-100 for 30 minutes. For myosin heavy chain skeletal muscle immunostaining, fish were blocked overnight at 4°C in 1x PBS 1% Triton X-100/ 5% NGS/ 10% DMSO. Anti-Myh (myosin heavy chain) monoclonal antibody (DSHB Hybridoma Product MF-20) was used at 1:250 in blocking solution overnight at 4°C and visualized with Alexa Fluor 647 anti-mouse secondary antibody (Thermo Fisher). Specimens were mounted on a FluroDish in SlowFade Gold prior to imaging.

Imaging

Alcian Blue and Alizarin Red stained fish were observed using a Leica M165 FC stereomicroscope equipped with a Leica DFC425 C camera. Widefield images of *trps1:EGFP* and *sox10:mRFP* larval transgenic fish were acquired on the same stereomicroscope. Confocal images of larval transgenic *trps1:EGFP*, *sox10:mRFP*, *sox9a:EGFP* were acquired on a Zeiss LSM5 Pascal confocal. A Nikon Eclipse T*i* microscope equipped with a Yokogawa CSU-W1 spinning disk confocal attachment was used to observe larval transgenic *RUNX2:mCherry;sp7:EGFP, alx4a:DsRed2* fish and MF-20 immunostained specimens. For longitudinal tracking of individual *RUNX2:mCherry;sp7:EGFP* larvae, *n=5* larvae were singly housed in petri dishes in standard nursery conditions and imaged 2-3x daily from 7-11 dpf until all principal fin rays developed, then 1x daily until 16 dpf. For expression profiling of *alx4a:DsRed2* fish, a group of *n=6* larvae were housed together in standard nursery conditions and imaged 1x daily from 12-16 dpf. Additional *alx4a:DsRed2* and *scxa:mCherry* fluorescent images in juveniles were captured using a Leica DMi8 equipped with an Andor Dragonfly 301 spinning disk confocal system. All confocal images are maximum intensity projections of sagittal Z-stacks.

Supplementary Material

Refer to Web version on PubMed Central for supplementary material.

Acknowledgments

We thank Tim Mason, John Dowd, and other staff at the University of Oregon AqACS Facility for zebrafish care, and the University of Oregon zebrafish community for support. This work was funded by NIH F31 GM139343 (AER), NSF GRFP 201569 (RBZ), NIH K99/R00 DE024190 and R01 DE029193 (JTN), NIH R01 OD011116 (JHP), and NIH R01 GM127761 (KS).

References

1. Giammona FF. Form and Function of the Caudal Fin Throughout the Phylogeny of Fishes. Integrative and Comparative Biology. 2021;61(2):550–572. doi:10.1093/icb/icab127 [PubMed: 34114010]
2. Gosline WA. Functional morphology of the caudal skeleton in teleostean fishes. Ichthyological Research. 1997;44(2–3):137–141. doi:10.1007/BF02678693
3. Lauder GV. Function of the Caudal Fin During Locomotion in Fishes: Kinematics, Flow Visualization, and Evolutionary Patterns. American Zoologist. 2000;40(1):101–122. doi:10.1668/0003-1569(2000)040[0101:FOTCFD]2.0.CO;2
4. Schultze HP, Arratia G. The composition of the caudal skeleton of teleosts (Actinopterygil: Osteichthyes). Zoological Journal of the Linnean Society. 1989;97(3):189–231. doi:10.1111/j.1096-3642.1989.tb00547.x
5. Bensimon-Brito A, Cancela ML, Huysseune A, Witten PE. Vestiges, rudiments and fusion events: the zebrafish caudal fin endoskeleton in an evo-devo perspective. Evol Dev. 2012;14(1):116–127. doi:10.1111/j.1525-142X.2011.00526.x [PubMed: 23016979]
6. Desvignes T, Carey A, Postlethwait JH. Evolution of caudal fin ray development and caudal fin hypural diastema complex in spotted gar, teleosts, and other neopterygian fishes. Developmental Dynamics. 2018;247(6):832–853. doi:10.1002/dvdy.24630 [PubMed: 29569346]
7. Arratia G Actinopterygian postcranial skeleton with special reference to the diversity of fin ray elements, and the problem of identifying homologies. In: Arratia G, Schultze HP, Wilson MVH, eds. Mesozoic Fishes 4 – Homology and Phylogeny. Verlag Dr. Friedrich Pfeil; 2008:49–101.

8. Arratia G Complexities of Early Teleostei and the Evolution of Particular Morphological Structures through Time. Copeia. 2015;103(4):999–1025. doi:10.1643/CG-14-184
9. Fricke R. A method of counting caudal fin rays of actinopterygian fishes. Braunschweiger Naturkundliche Schriften. 1983;1(4):729–733.
10. Schultze HP, Arratia G. The caudal skeleton of basal teleosts, its conventions, and some of its major evolutionary novelties in a temporal dimension. In: Wilson MVH, Arratia G, Schultze HP, eds. Mesozoic Fishes 5 - Global Diversity and Evolution. München: F. Pfeil; 2013:187–246.
11. Bird NC, Mabee PM. Developmental morphology of the axial skeleton of the zebrafish, Danio rerio (Ostariophysi: Cyprinidae). Dev Dyn. 2003;228(3):337–357. doi:10.1002/dvdy.10387 [PubMed: 14579374]
12. Fujita K Caudal skeleton ontogeny in the adrianichthyid fish,Oryzias latipes. Japanese Journal of Ichthyology. 1992;39(1):107–109. doi:10.1007/BF02905639
13. Huxley TH. Observations on the Development of some parts of the Skeleton of Fishes. Transactions of The Microscopical Society & Journal. 1859;7(1):33–46. doi:10.1111/j.1365-2818.1859.tb04575.x
14. Konstantinidis P, Johnson GD. A comparative ontogenetic study of the tetraodontiform caudal complex: Caudal complex of tetraodontiforms. Acta Zoologica. 2012;93(1):98–114. doi:10.1111/j.1463-6395.2010.00490.x
15. Li IJ, Chang CJ, Liu SC, Abe G, Ota KG. Postembryonic staging of wild-type goldfish, with brief reference to skeletal systems. Developmental Dynamics. 2015;244(12):1485–1518. doi:10.1002/dvdy.24340 [PubMed: 26316229]
16. Thieme P, Warth P, Moritz T. Development of the caudal-fin skeleton reveals multiple convergent fusions within Atherinomorpha. Frontiers in Zoology. 2021;18(1):20. doi:10.1186/s12983-021-00408-x [PubMed: 33902629]
17. Desvignes T, Carey A, Braasch I, Enright T, Postlethwait JH. Skeletal development in the heterocercal caudal fin of spotted gar (lepisosteus oculatus) and other lepisosteiformes. Developmental Dynamics. 2018;247(5):724–740. doi:10.1002/dvdy.24617 [PubMed: 29330942]
18. Kirby BB, Takada N, Latimer AJ, et al. In vivo time-lapse imaging shows dynamic oligodendrocyte progenitor behavior during zebrafish development. Nature Neuroscience. 2006;9(12):1506–1511. doi:10.1038/nn1803 [PubMed: 17099706]
19. Talbot JC, Johnson SL, Kimmel CB. hand2 and Dlx genes specify dorsal, intermediate and ventral domains within zebrafish pharyngeal arches. Development. 2010;137(15):2507–2517. doi:10.1242/dev.049700 [PubMed: 20573696]
20. Eames BF, DeLaurier A, Ullmann B, et al. FishFace: interactive atlas of zebrafish craniofacial development at cellular resolution. BMC Developmental Biology. 2013;13(1):23. doi:10.1186/1471-213X-13-23 [PubMed: 23714426]
21. Barske L, Fabian P, Hirschberger C, et al. Evolution of vertebrate gill covers via shifts in an ancient Pou3f3 enhancer. PNAS. 2020;117(40):24876–24884. doi:10.1073/pnas.2011531117 [PubMed: 32958671]
22. DeLaurier A, Eames BF, Blanco-Sanchez B, et al. Zebrafish sp7:EGFP: a transgenic for studying otic vesicle formation, skeletogenesis, and bone regeneration. Genesis. 2010;48(8):505–511. doi:10.1002/dvg.20639 [PubMed: 20506187]
23. Komori T Regulation of Proliferation, Differentiation and Functions of Osteoblasts by Runx2. International Journal of Molecular Sciences. 2019;20(7):1694. doi:10.3390/ijms20071694
24. Sinha KM, Zhou X. Genetic and molecular control of osterix in skeletal formation. Journal of Cellular Biochemistry. 2013;114(5):975–984. doi:10.1002/jcb.24439 [PubMed: 23225263]
25. Stewart S, Gomez AW, Armstrong BE, Henner A, Stankunas K. Sequential and Opposing Activities of Wnt and BMP Coordinate Zebrafish Bone Regeneration. Cell Reports. 2014;6(3):482–498. doi:10.1016/j.celrep.2014.01.010 [PubMed: 24485659]
26. Nachtrab G, Kikuchi K, Tornini VA, Poss KD. Transcriptional components of anteroposterior positional information during zebrafish fin regeneration. Development. 2013;140(18):3754–3764. doi:10.1242/dev.098798 [PubMed: 23924636]

27. Jang HS, Chen Y, Ge J, et al. Epigenetic dynamics shaping melanophore and iridophore cell fate in zebrafish. Genome Biology. 2021;22(1):282. doi:10.1186/s13059-021-02493-x [PubMed: 34607603]
28. Parichy DM, Elizondo MR, Mills MG, Gordon TN, Engeszer RE. Normal table of postembryonic zebrafish development: Staging by externally visible anatomy of the living fish. Dev Dyn. 2009;238(12):2975–3015. doi:10.1002/dvdy.22113 [PubMed: 19891001]
29. Siomava N, Shkil F, Voronezhskaya E, Diogo R. Development of zebrafish paired and median fin musculature: basis for comparative, developmental, and macroevolutionary studies. Scientific Reports. 2018;8(1):14187. doi:10.1038/s41598-018-32567-z [PubMed: 30242203]
30. Chen JW, Galloway JL. The development of zebrafish tendon and ligament progenitors. Development. 2014;141(10):2035–2045. doi:10.1242/dev.104067 [PubMed: 24803652]
31. Kague E, Hughes SM, Lawrence EA, et al. Scleraxis genes are required for normal musculoskeletal development and for rib growth and mineralization in zebrafish. The FASEB Journal. 2019;33(8):9116–9130. doi:10.1096/fj.201802654RR [PubMed: 31100023]
32. McGurk PD, Swartz ME, Chen JW, Galloway JL, Eberhart JK. In vivo zebrafish morphogenesis shows Cyp26b1 promotes tendon condensation and musculoskeletal patterning in the embryonic jaw. PLOS Genetics. 2017;13(12):e1007112. doi:10.1371/journal.pgen.1007112 [PubMed: 29227993]
33. Wiley EO, Fuiten AM, Doosey MH, Lohman BK, Merkes C, Azuma M. The Caudal Skeleton of the Zebrafish, Danio rerio, from a Phylogenetic Perspective: A Polyural Interpretation of Homologous Structures. Copeia. 2015;103(4):740–750. doi:10.1643/CG-14-105 [PubMed: 28250540]
34. Hadzhiev Y, Lele Z, Schindler S, et al. Hedgehog signaling patterns the outgrowth of unpaired skeletal appendages in zebrafish. BMC Developmental Biology. 2007;7(1):75. doi:10.1186/1471-213X-7-75 [PubMed: 17597528]
35. Bump RG, Goo CEA, Horton EC, Rasmussen JP. Osteoblasts pattern endothelium and somatosensory axons during zebrafish caudal fin organogenesis. Development. 2022;149(3):dev200172. doi:10.1242/dev.200172 [PubMed: 35129199]
36. Iida Y, Hibiya K, Inohaya K, Kudo A. Eda/Edar signaling guides fin ray formation with preceding osteoblast differentiation, as revealed by analyses of the medaka all-fin less mutant afl. Developmental Dynamics. 2014;243(6):765–777. doi:10.1002/dvdy.24120 [PubMed: 24585696]
37. Onimaru K, Marcon L, Musy M, Tanaka M, Sharpe J. The fin-to-limb transition as the re-organization of a Turing pattern. Nat Commun. 2016;7(1):11582. doi:10.1038/ncomms11582 [PubMed: 27211489]
38. Raspopovic J, Marcon L, Russo L, Sharpe J. Digit patterning is controlled by a Bmp-Sox9-Wnt Turing network modulated by morphogen gradients. Science. August 2014. doi:10.1126/science.1252960
39. Stewart S, Yette GA, Bleu HKL, et al. Skeletal Geometry and Niche Transitions Restore Organ Size and Shape during Zebrafish Fin Regeneration; 2019:606970. doi:10.1101/606970
40. Nichols JT, Blanco-Sánchez B, Brooks EP, et al. Ligament versus bone cell identity in the zebrafish hyoid skeleton is regulated by mef2ca. Development. 2016;143(23):4430–4440. doi:10.1242/dev.141036 [PubMed: 27789622]
41. Flammang BE, Lauder GV. Speed-dependent intrinsic caudal fin muscle recruitment during steady swimming in bluegill sunfish, Lepomis macrochirus. Journal of Experimental Biology. 2008;211(4):587–598. doi:10.1242/jeb.012096 [PubMed: 18245636]
42. Flammang BE, Lauder GV. Caudal fin shape modulation and control during acceleration, braking and backing maneuvers in bluegill sunfish, Lepomis macrochirus. Journal of Experimental Biology. 2009;212(2):277–286. doi:10.1242/jeb.021360 [PubMed: 19112147]
43. Esposito CJ, Tangorra JL, Flammang BE, Lauder GV. A robotic fish caudal fin: effects of stiffness and motor program on locomotor performance. Journal of Experimental Biology. 2012;215(1):56–67. doi:10.1242/jeb.062711 [PubMed: 22162853]
44. Luo Y, Xiao Q, Shi G, Wen L, Chen D, Pan G. A fluid–structure interaction solver for the study on a passively deformed fish fin with non-uniformly distributed stiffness. Journal of Fluids and Structures. 2020;92:102778. doi:10.1016/j.jfluidstructs.2019.102778

45. Shi G, Xiao Q, Zhu Q, Liao W. Fluid-structure interaction modeling on a 3D ray-strengthened caudal fin. Bioinspir Biomim. 2019;14(3):036012. doi:10.1088/1748-3190/ab0fbe [PubMed: 30870830]
46. Morphology Arratia G., Taxonomy, and Phylogeny of Triassic Pholidophorid Fishes (Actinopterygii, Teleostei). Journal of Vertebrate Paleontology. 2013;33(S1):1–138. doi:10.1080/02724634.2013.835642
47. Metscher BD, Ahlberg PE. Origin of the teleost tail: phylogenetic frameworks for developmental studies. In: Ahlberg PE, Systematics Association, eds. Major Events in Early Vertebrate Evolution: Palaeontology, Phylogeny, Genetics, and Development. London ; New York: Taylor & Francis; 2001:343–349.
48. Sallan L. Fish 'tails' result from outgrowth and reduction of two separate ancestral tails. Current Biology. 2016;26(23):R1224–R1225. doi:10.1016/j.cub.2016.10.036 [PubMed: 27923128]
49. Darwin C The Descent of Man, and Selection in Relation to Sex. John Murray; 1871. https://www.degruyter.com/document/doi/10.1515/9781400820061/html. Accessed May 26, 2021.
50. Eibner C, Pittlik S, Meyer A, Begemann G. An organizer controls the development of the "sword," a sexually selected trait in swordtail fish. Evolution & Development. 2008;10(4):403–412. doi:10.1111/j.1525-142X.2008.00251.x [PubMed: 18638317]
51. Schartl M, Kneitz S, Ormanns J, et al. The Developmental and Genetic Architecture of the Sexually Selected Male Ornament of Swordtails. Current Biology. 2021;31(5):911–922.e4. doi:10.1016/j.cub.2020.11.028 [PubMed: 33275891]
52. Davenport J. How and why do flying fish fly? Rev Fish Biol Fisheries. 1994;4(2):184–214. doi:10.1007/BF00044128
53. Davis MP, Chakrabarty P. Tripodfish (Aulopiformes: Bathypterois) locomotion and landing behaviour from video observation at bathypelagic depths in the Campos Basin of Brazil. Marine Biology Research. 2011;7(3):297–303. doi:10.1080/17451000.2010.515231
54. Paixão A de C, Toledo-Piza M. Systematics of Lamontichthys Miranda-Ribeiro (Siluriformes: Loricariidae), with the description of two new species. Neotrop ichthyol. 2009;7:519–568. doi:10.1590/S1679-62252009000400002
55. Rojas-Molina YA, Provenzano-Rizzi F, Ramírez-Gil H. A new species of whiptail armored catfish, genus Pseudohemiodon (Siluriformes: Loricariidae) from the Orinoco River basin, Llanos region of Colombia and Venezuela. Neotrop ichthyol. 2019;17. doi:10.1590/1982-0224-20180160
56. Terán GE, Ballen GA, Alonso F, Aguilera G, Mirande JM. A new species of Farlowella (Siluriformes: Loricariidae) from the upper Bermejo River, La Plata River basin, northwestern Argentina. Neotrop ichthyol. 2019;17. doi:10.1590/1982-0224-20180114
57. Thomas MR, Pérez MHS. A New Species of Whiptail Catfish, Genus Loricaria (Siluriformes: Loricariidae), from the Rio Curuá (Xingu Basin), Brazil. cope. 2010;2010(2):274–283. doi:10.1643/CI-09-097
58. Daane JM, Blum N, Lanni J, et al. Modulation of bioelectric cues in the evolution of flying fishes. Current Biology. September 2021. doi:10.1016/j.cub.2021.08.054
59. Stewart S, Le Bleu HK, Yette GA, et al. longfin causes cis-ectopic expression of the kcnh2a ether-a-go-go K+ channel to autonomously prolong fin outgrowth. Development. 2021;(dev.199384). doi:10.1242/dev.199384
60. Perathoner S, Daane JM, Henrion U, et al. Bioelectric Signaling Regulates Size in Zebrafish Fins. PLOS Genet. 2014;10(1):e1004080. doi:10.1371/journal.pgen.1004080 [PubMed: 24453984]
61. Kon T, Omori Y, Fukuta K, et al. The Genetic Basis of Morphological Diversity in Domesticated Goldfish. Current Biology. 2020;30(12):2260–2274.e6. doi:10.1016/j.cub.2020.04.034 [PubMed: 32392470]
62. Silic MR, Wu Q, Kim BH, et al. Potassium Channel-Associated Bioelectricity of the Dermomyotome Determines Fin Patterning in Zebrafish. Genetics. 2020;215(4):1067–1084. doi:10.1534/genetics.120.303390 [PubMed: 32546498]
63. Schneider CA, Rasband WS, Eliceiri KW. NIH Image to ImageJ: 25 years of image analysis. Nature Methods. 2012;9(7):671–675. doi:10.1038/nmeth.2089 [PubMed: 22930834]

64. Kimmel CB, Ballard WW, Kimmel SR, Ullmann B, Schilling TF. Stages of embryonic development of the zebrafish. Developmental Dynamics. 1995;203(3):253–310. doi:10.1002/aja.1002030302 [PubMed: 8589427]

65. Walker M, Kimmel C. A two-color acid-free cartilage and bone stain for zebrafish larvae. Biotechnic & Histochemistry. 2007;82(1):23–28. doi:10.1080/10520290701333558 [PubMed: 17510811]

Key findings

1. A central hypural diastema organizing center (HDOC) patterns a gap in the caudal fin between hypurals 2 and 3 and develops prior to more distal skeletal elements.
2. The caudal fin's plates of connective tissue and dorsoventrally mirrored sets of central principal rays (CPRs) emerge symmetrically and synchronously around the HDOC.
3. Two sets of two peripheral principal rays (PPRs) form asynchronously from the CPRs at dorsal and ventral fin lobe edges, suggesting two separate peripheral organizing centers (POCs).
4. Each set of CPR and PPR rays attaches to different swimming muscles.
5. The HDOC and two POCs may represent three developmental modules that collectively produce external symmetry and underlie teleost caudal fin shape variation.

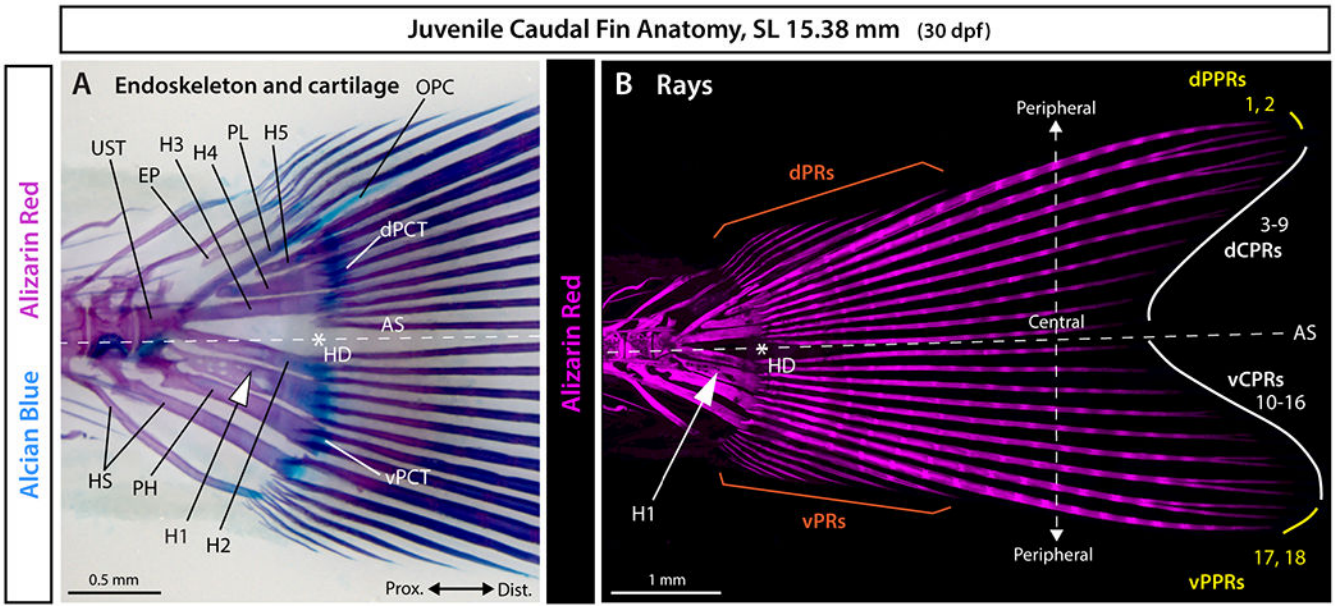

Figure 1. Anatomy of the zebrafish caudal skeleton.

A: Whole mount brightfield and **B:** maximum intensity projection of confocal fluorescent images of a juvenile zebrafish caudal fin stained with Alcian Blue and Alizarin Red. The white asterisk denotes the hypural diastema (HD), the white arrowhead indicates the hypural 1 (H1), and the white dashed line marks the axis of external dorsoventral symmetry (AS). Abbreviations: dCPRs and vCPRs (white), dorsal and ventral central principal rays, respectively; dPCT and vPCT, dorsal and ventral plates of connective tissue, respectively; dPPRs and vPPRs (yellow), dorsal and ventral peripheral principal rays, respectively; dPRs and vPRs (orange), dorsal and ventral procurrent rays, respectively; EP, epural; H1-H5, hypurals 1 to 5; HS, haemal spine; OPC, opisthural cartilage; PH, parhypural; PL, pleurostyle; UST, urostyle.

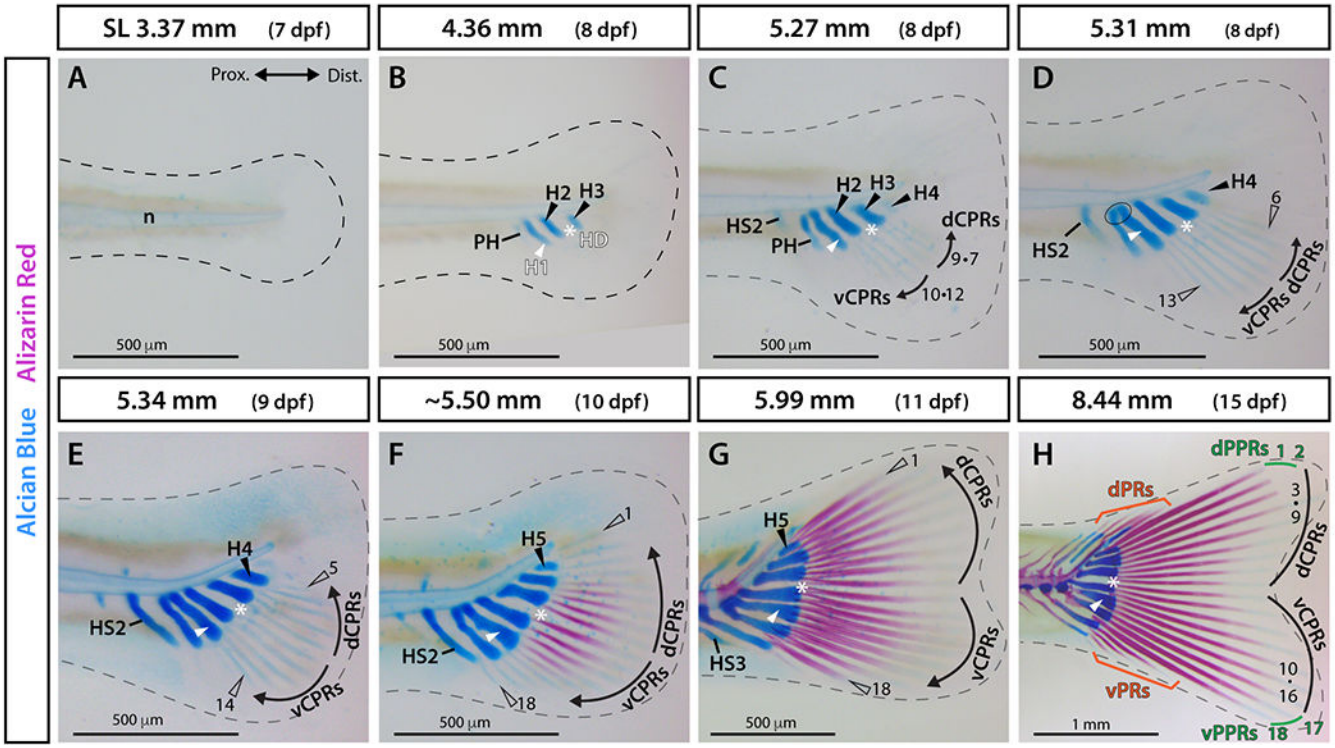

Figure 2. Alcian Blue and Alizarin Red visualization of caudal fin symmetry establishment and body axis alignment anchored by the hypural diastema.

A-H: Whole-mount images of Alcian Blue (cartilage) and Alizarin Red (calcified bone) stained caudal fin skeletons across a zebrafish larval developmental sequence. The dashed line marks the border of the fin fold. The ellipse in D indicates fusion of the parhypural and hypural 1. Abbreviations: dCPRs and vCPRs, dorsal and ventral central principal rays, respectively (black); dPPRs and vPPRs, dorsal and ventral peripheral principal rays, respectively (green); dPRs and vPRs, dorsal and ventral procurrent rays, respectively (orange); H1 and white arrowhead, hypural 1; H2-5 and black arrowheads, hypurals 2 to 5; HD and white asterisk, hypural diastema; HS2-3, haemal spines 2 and 3; n, notochord; PH, parhypural.

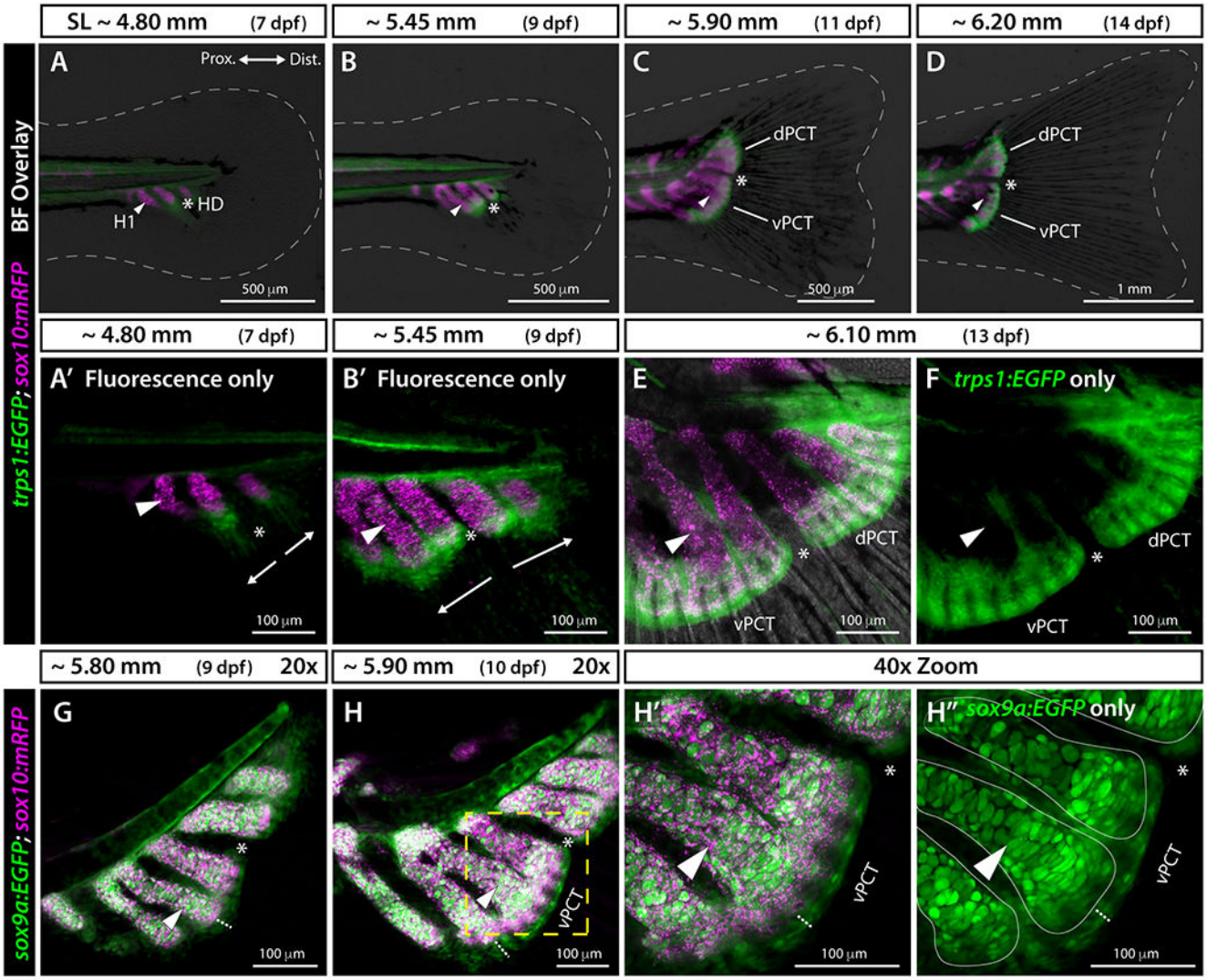

Figure 3. Transgenic reporters reveal that plates of connective tissue develop symmetrically around the hypural diastema.

A-D: Widefield and **A', B', E, F:** confocal whole mount images of the caudal region of *trps1:EGFP*;*sox10:mRFP* larval zebrafish. White dashed line indicates fin boundaries. *sox10:mRFP* labels endochondral elements including hypurals, parhypural, and haemal spines, and *trps1:EGFP* labels precursor cells of the two plates of connective tissue. The hypural diastema lies between hypurals 2 and 3 and separates the two developing plates of connective tissue. Arrows in A' and B' indicate the directions of outgrowth of the plates of connective tissue. **G-H":** Confocal images of *sox9a:EGFP*;*sox10:mRFP* larval zebrafish. *sox9a:EGFP* and *sox10:mRFP* transgenes are co-expressed in endochondral elements with additional *sox9a:EGFP* expression in the two developing plates of connective tissue separated at the hypural diastema. The white dotted lines in H-H'' show the thickness of the plates of connective tissue. The yellow dashed line in H is blown up in H' and H". Solid thin white lines in H" denote the borders of the endochondral skeletal elements

based on H'. Abbreviations: dPCT and vPCT, dorsal and ventral plates of connective tissue, respectively; H1 and white arrowhead, Hypural 1; HD and white asterisk, hypural diastema.

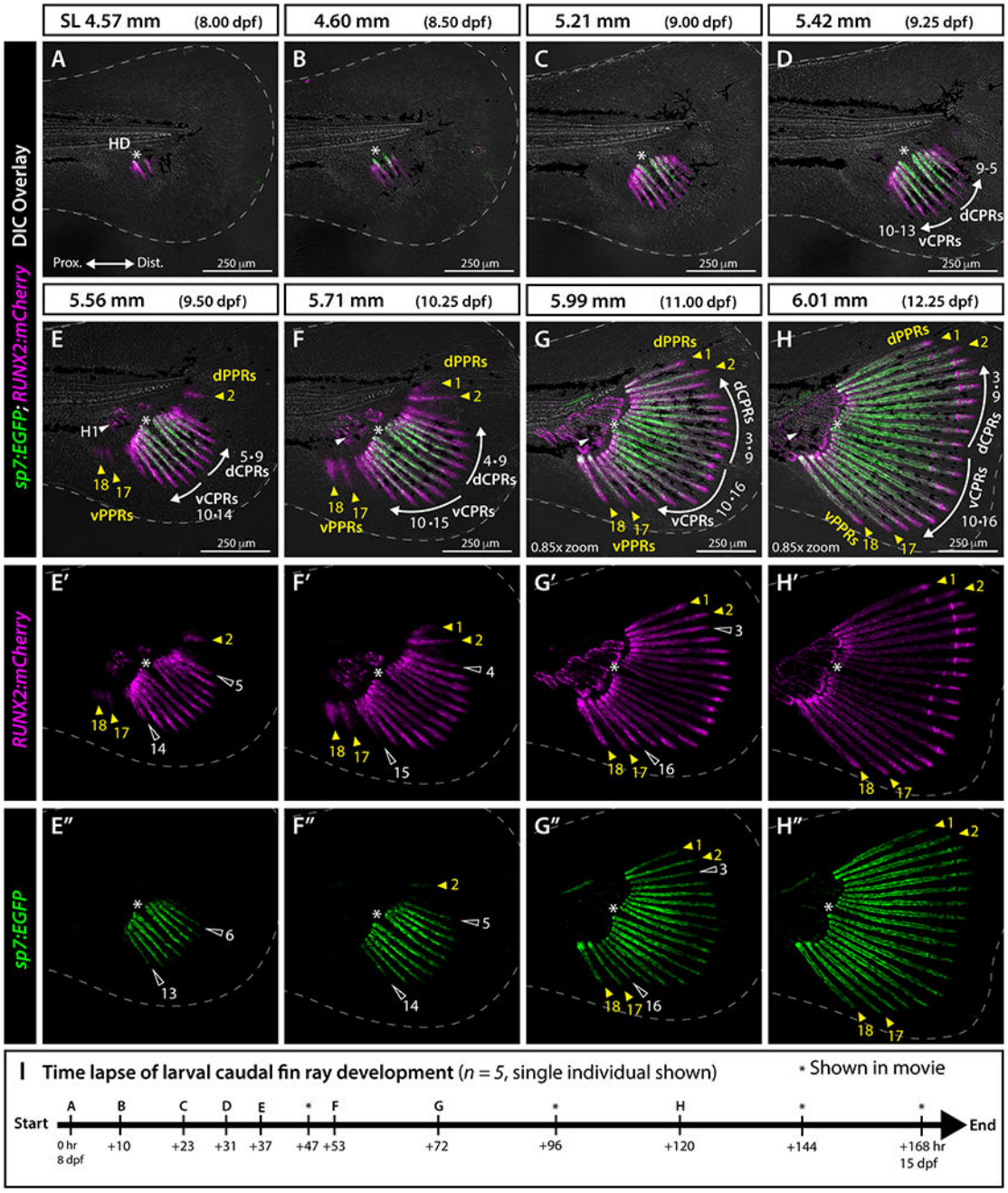

Figure 4. Osteoblast developmental state markers demonstrate synchronous and symmetric central principal ray formation and distinct emergence of peripheral principal caudal fin rays.

A-H": Whole mount confocal images of a representative *RUNX2:mCherry;sp7:EGFP* larva (from $n = 5$) followed from SL 4.57 mm to 6.01 mm (8-12.25 dpf) and imaged following the schedule in I. Differential interference contrast (DIC) overlayed in A-H; *RUNX2:mCherry* (pre-osteoblasts, magenta) single channel in E'-H'; and *sp7:EGFP* (differentiating osteoblasts, green) single channel in E"-H". White dashed line indicates fin boundaries. Central principal ray directions of outgrowth are indicated by white arrows

in D-H. Abbreviations: dCPRs and vCPRs, dorsal and ventral central principal rays, respectively; dPPRs and vPPRs, dorsal and ventral peripheral principal rays, respectively (yellow arrowheads); H1 and white arrowhead, hypural 1; HD and white asterisk, hypural diastema. **I:** Timing of time lapse image acquisition points shown in the corresponding panels (letters) and additionally in Video S1 (asterisks).

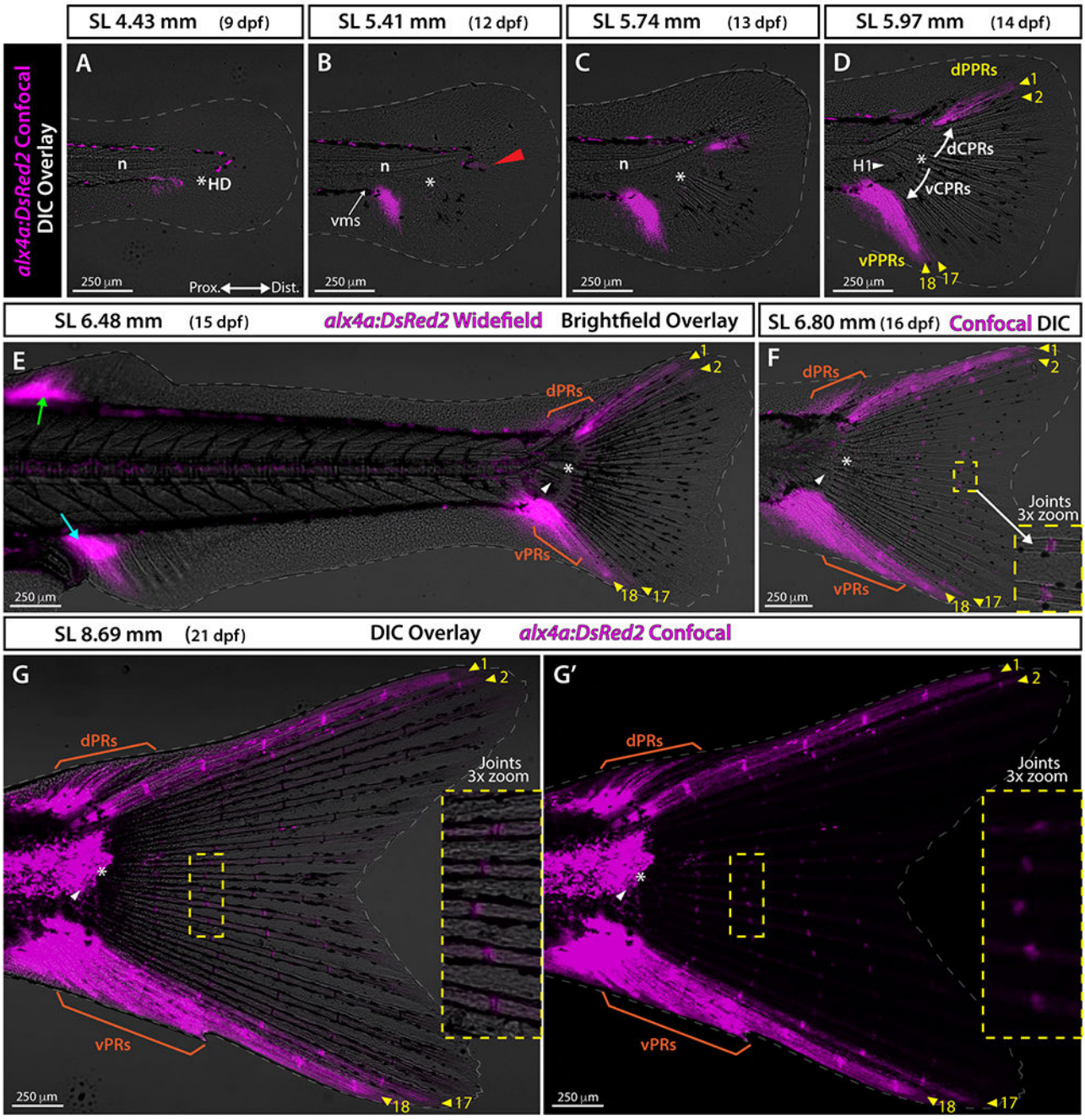

Figure 5. alx4a transgenic expression indicates the distinct nature of peripheral principal rays. **A-D** and **F-G:** Confocal images overlaid with differential interference contrast (DIC). **E:** Widefield fluorescence image with brightfield overlaid. Gray dashed line indicates fin boundaries. **G':** *alx4a:DsRed2* expression in G shown in single channel. Red arrowhead in B points at the faint *alx4a:DsRed2* expression just below the notochord distal tip. White arrows in D mark the sequence of central principal ray specification. Green and cyan arrows in E point at the *alx4a:DsRed2* expression at the leading rays of the dorsal and anal fins, respectively. Abbreviations: dCPRs and vCPRs, dorsal and ventral central principal

rays; dPPRs and vPPRs, dorsal and ventral peripheral principal rays, respectively (yellow arrowheads); dPRs and vPRs, dorsal and ventral procurrent rays, respectively (orange); H1 and white arrowhead, Hypural 1; HD and white asterisk, hypural diastema; n, notochord; vms, ventral melanophore stripe before the caudal fin condensation region.

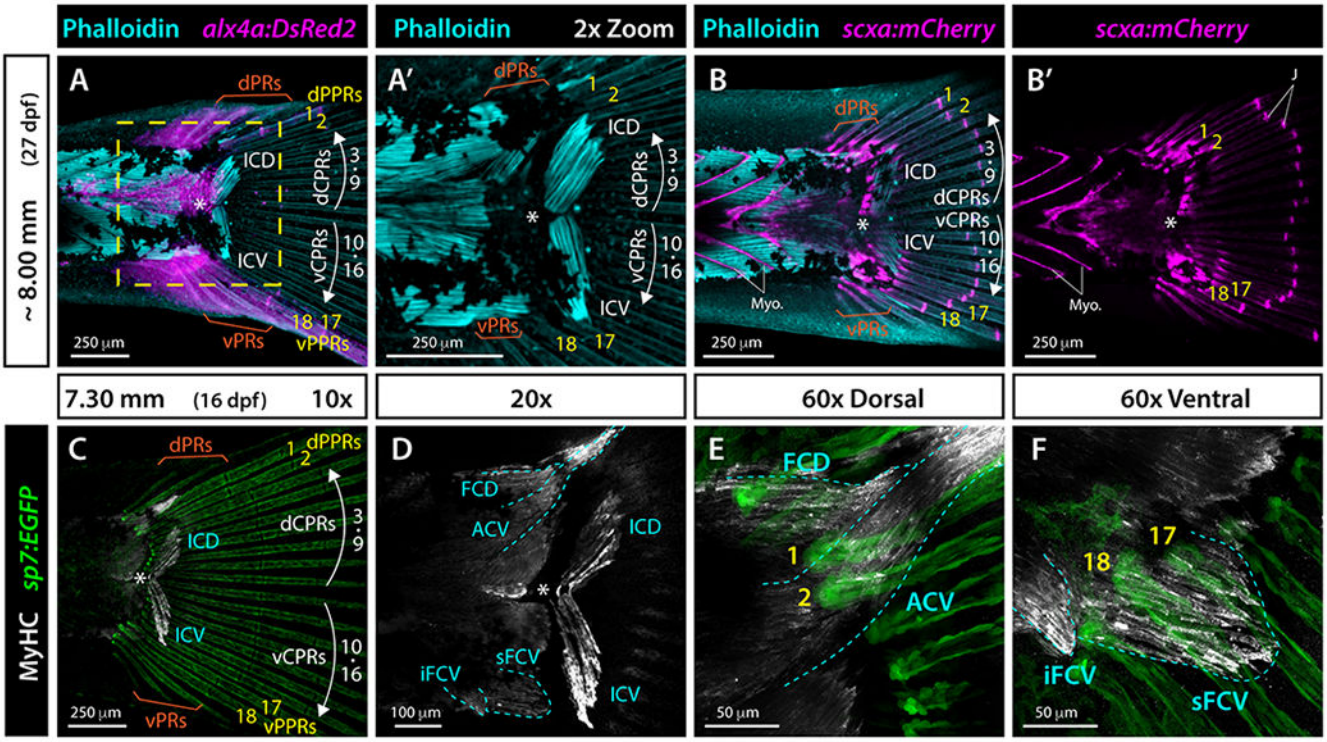

Figure 6. Muscle staining combined with alx4a and scxa reporters reveal that each set of central principal rays and peripheral principal rays is associated with distinct swimming muscles.

Whole mount widefield fluorescent images of the caudal region of zebrafish larvae. **A, A':** Phalloidin-stained ~8.00 mm *alx4a:DsRed2* larval zebrafish. F-actin (phalloidin) is cyan and *alx4a:DsRed2*-expressing cells, including peripheral principal rays (PPRs), are magenta. **B-B':** Phalloidin-stained (cyan) ~8.00 mm *scxa:mCherry* larval zebrafish. The mCherry fluorescent marker (magenta) labels tendons, myosepta, and caudal fin ray joints. **C-F:** Whole mount immunostained 7.30 mm *sp7:EGFP* (green) larva. Myosin heavy chain (Myh) antibody labels skeletal muscles (white). EGFP fluorescence is green. Muscles are outlines in cyan dashed line. Abbreviations: ACV, abductor caudalis ventralis; dCPR and vCPR, dorsal and ventral central principal rays, respectively; dPPR and vPPR (yellow), dorsal and ventral peripheral principal rays, respectively; dPR and vPR, dorsal and ventral procurrent rays, respectively; FCD, flexor caudalis dorsalis; ICD, inerfilamenti caudalis dorsalis; ICV, inerfilamenti caudalis ventralis; iFCV, inferior flexor caudalis ventralis; J, ray joints; Myo, myosepta; sFCV, superior flexor caudalis ventralis; white asterisk, hypural diastema.

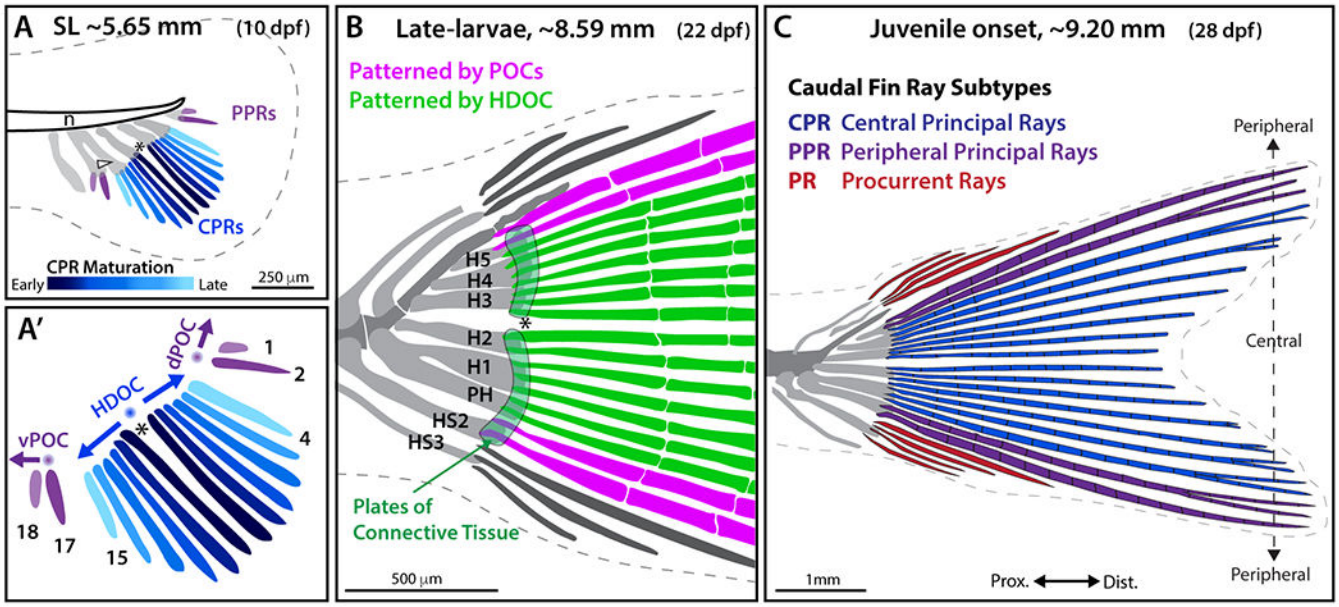

Figure 7. Schematic representation of zebrafish caudal fin skeletal patterning.

The caudal fin comprises three subtypes of fin rays differing in their ontogeny, morphology, and identity: central principal rays (CPRs), two sets of peripheral principal rays (ventral and dorsal PPRs), and procurrent rays (PRs). **A-A':** CPRs (blue, with dark-to-light color gradient representing the first-to-last forming rays) are specified by a hypothetical bidirectional hypural diastema organizing center (HDOC; blue sphere) triggering the sequential and synchronous addition of mirrored pairs of rays (14 total) symmetrically distributed around the hypural diastema (asterisk). Two sets of PPRs (principal rays 1, 2 and 17, 18; purple) develop separately from the CPRs, unidirectionally specified by two hypothetical peripheral organizing centers (POCs, purple spheres). **(B)** Two plates of connective tissue (light green) are specified on each side of the HDOC along with CPRs (green), while PPRs (pink) are specified by POCs. H1-H5, Hypurals 1-5; HS2 and HS3, haemal spines 2 and 3. **(C)** CPRs (blue) are segmented and branched. Among PPRs (purple), the two most peripheral (principal rays 1 and 18) are segmented but unbranched, while PPR 2 and 17 are segmented and branched. Unbranched PRs (red) emerge after the formation of all principal rays. This model proposes that the caudal fin is a "compound" appendage with body axis-aligned external symmetry arising from 1) HDOC-initiated, symmetrically specified CPRs and plates of connective tissue, 2) two similar PPR sets specified by two POCs equally spaced from the HDOC, and 3) upward bending of the notochord that rotates skeletal elements from an anterior-posterior to a dorsal-ventral position, aligning the hypural diastema with the body axis.